Inorg. Chem. **2003**, *42*, 4660–4667

Inorganic Chemistry
Article

$Eu_{10}Mn_6Sb_{13}$: A New Ternary Rare-Earth Transition-Metal Zintl Phase

**Aaron P. Holm,[†] Seon-Mi Park,[‡] Cathie L. Condron,[†] Marilyn M. Olmstead,[†] Hyungrak Kim,[†]
Peter Klavins,[§] Fernande Grandjean,*,[||] Raphaël P. Hermann,[||] Gary J. Long,*,[⊥]
Mercouri G. Kanatzidis,[¶] Susan M. Kauzlarich,*,[†] and Sung-Jin Kim*,[‡]**

*Departments of Chemistry and Physics, University of California, One Shields Avenue,
Davis, California 95616, Department of Chemistry, Ewha Womans University,
Seoul, Korea, 120-750, Institute of Physics, B5, University of Liège, B-4000 Sart-Tilman, Belgium,
Department of Chemistry, University of Missouri—Rolla, Rolla, Missouri 65409-0010, and
Department of Chemistry and Center for Fundamental Materials Research, Michigan State
University, East Lansing, Michigan 48824*

Received January 18, 2003

A new transition-metal-containing Zintl compound, $Eu_{10}Mn_6Sb_{13}$, was prepared by a high-temperature Sn-flux synthesis. The structure was determined by single-crystal X-ray diffraction. $Eu_{10}Mn_6Sb_{13}$ crystallizes in the monoclinic space group $C2/m$ with $a = 15.1791(6)$ Å, $b = 19.1919(7)$ Å, $c = 12.2679(4)$ Å, $\beta = 108.078(1)°$, $Z = 4$ (R1 = 0.0410, wR2 = 0.0920), and $T = 90(2)$ K. The structure of $Eu_{10}Mn_6Sb_{13}$ is composed of double layers of Mn-centered tetrahedra separated by Eu^{2+} cations. The double layers are composed of edge- and corner-sharing Mn-centered tetrahedra which form cavities occupied by Eu^{2+} cations and $[Sb_2]^{4-}$ dumbbells. Linear $[Sb_3]^{5-}$ trimers bridging two tetrahedra across the cavity are also present. Bulk susceptibility data indicate paramagnetic behavior with a ferromagnetic component present below 60 K. Temperature-dependent electrical resistivity measurements show semiconducting behavior above 60 K ($E_a = 0.115(2)$ eV), a large and unusually sharp maximum in the resistivity at ∼40 K, and metallic behavior below 40 K. ^{151}Eu Mössbauer spectra confirm that the europium is divalent with an average isomer shift of –11.2(1) mm/s at 100 K; the spectra obtained below 40 K reveal magnetic ordering of six of the seven europium sublattices and, at 4.2 K, complete ordering of the seven europium sublattices.

Introduction

The correlation of increasing structural complexity with the increasingly complex physical properties of intermetallic phases has motivated our search for new transition-metal Zintl phases possessing unique magnetic and electronic properties.[1–3] Recent reports on the new thermoelectric materials $CsBi_4Te_6$ and $Ba_4In_8Sb_{16}$ point to the unusual combination of complex electrical, structural, and thermal properties as a route toward a higher thermoelectric figure of merit.[2,3] In addition, superconductivity has been observed in the binary Zintl phases $BaSn_3$ ($T_C = 4.3$ K)[4] and $SrSn_3$ ($T_C = 5.4$ K),[5] the rare-earth gallium antimonide $La_{13}Ga_8Sb_{21}$ ($T_C = 2.4$ K),[6] and the ternary antimonides $Ba_2Sn_3Sb_6$ and $SrSn_3Sb_4$ ($T_C = 3.9$ K).[7] These results indicate that other Zintl compounds with complex bonding arrangements and lower electronegativity differences between the component atoms may also be superconductors. The structure types of many Zintl phases also have potential as design guides in the burgeoning field of molecule-based magnets in which the solid-state magnetic structures often consist of arrays of molecular units similar to the typical Zintl phase.[8,9] The complexity inherent in the electronic and crystal structures of Zintl phases has led to the discovery of new compounds

---

* Authors to whom correspondence should be addressed. E-mail: sjkim@ewha.ac.kr (S.-J.K.); smkauzlarich@ucd.edu (S.M.K.); fgrandjean@ulg.ac.be (F.G.); glong@umr.edu (G.J.L.).

[†] Department of Chemistry, University of California.

[‡] Ewha Womans University.

[§] Department of Physics, University of California.

[||] University of Liège.

[⊥] University of Missouri—Rolla.

[¶] Michigan State University.

(1) Kauzlarich, S. M.; Payne, A. C.; Webb, D. J. In *Magnetism: Molecules to Materials III*; Miller, J. S., Drillon, M., Eds.; Wiley-VCH: Weinheim, Germany, 2002; pp 37–62.

(2) Kim, S.-J.; Hu, S.; Uher, C.; Kanatzidis, M. G. *Chem. Mater.* **1999**, *11*, 3154–3159.

(3) Chung, D.-Y.; Hogan, T.; Brazis, P.; Rocci-Lane, M.; Kannewurf, C.; Bastea, M.; Uher, C.; Kanatzidis, M. G. *Science* **2000**, *287*, 1024–1027.

(4) Fässler, T. F.; Hoffmann, S.; Kronseder, C. *Z. Anorg. Allg. Chem.* **2001**, *627*, 2486-2492.

(5) Fässler, T. F.; Hoffmann, S. *Z. Anorg. Allg. Chem.* **2000**, *626*, 106–112.

(6) Mills, A. M.; Deakin, L.; Mar, A. *Chem. Mater.* **2001**, *13*, 1778–1788.

(7) Deakin, L.; Lam, R.; Marsiglio, F.; Mar, A. *J. Alloys Compd.* **2002**, *388*, 69–72.

10.1021/ic034054w CCC: $25.00

with large magnetoresistive effects. Most notably colossal magnetoresistance has been reported[1,10−15] in the $A_{14}MnPn_{11}$ compounds, where A is Ca, Sr, Ba, Eu, or Yb and Pn is P, As, Sb, or Bi.

The structural diversity of Zintl compounds at the metal−insulator boundary can often be simplified by identifying the basic structural units or motifs, which in many cases can help in providing a prediction of a compound's bulk properties. The presence of a layered crystal structure is often an indication of interesting physical properties such as superconductivity, high charge transport anisotropy, colossal magnetoresistance, or charge density waves due to the two-dimensional structure of functional sublattices.[16] In addition, the combination of isolated structural units and an extended network have been identified as prerequisites for the occurrence of superconductivity as a result of the competition between the localization of electrons in the isolated units and delocalization in the extended networks.[5,6,17]

This paper reports on the new compound $Eu_{10}Mn_6Sb_{13}$, a further addition to the growing family of Mn-containing transition-metal Zintl compounds. The structure, magnetic, electric, and ^{151}Eu Mössbauer spectral properties are reported herein.

Experimental Section

Synthesis. The synthesis and crystal structure of $Eu_{10}Mn_6Sb_{13}$ have been independently investigated in both the UCD and the EWU laboratories. The crystal structures of the samples prepared in the two laboratories were found to be identical. The single crystals of $Eu_{10}Mn_6Sb_{13}$ were synthesized using Sn as a flux.[18] The mixture of elements (Eu:Mn:Sb:Sn = 10:6:13:30), Sn (Junsei, drops, 99.9%), Eu (Aldrich, chips, 99.9%), Mn (Aldrich, powder, 99.9%), and Sb (high purity, powder, 99.999%), was placed in a graphite tube, which was then vacuum-sealed in a fused silica tube. The mixture was heated to 1000 °C at a rate of 10 °C/h, held at 1000 °C for 24 h, cooled to 550 °C at 5 °C/h, held at 550 °C for 4 days, and then cooled to room temperature at 5 °C/h. The compound could also be prepared according to the following procedure. The mass of each element was scaled to 2.0 g of Sn according to the ratio 14:6:13:42 Eu:Mn:Sb:Sn (Eu (Ames Lab, 99.999%), Mn pieces (Alfa, 99.98%), Sb shot (CERAC, 99.999%) and Sn shot (Alfa, 99.99%)). The elements were layered into a 2 mL alumina crucible, placed into a fused silica tube with a second crucible filled with SiO_2 wool placed on top, and the fused silica tube was sealed under 0.2 atm of argon. The reaction vessel was placed upright in a box furnace and heated at 60 °C/h to 500 °C, allowed to dwell for 1 h, and then heated at 60 °C/h to 1100 °C. Subsequently, the reaction vessel was slowly cooled at 1 °C/h to 600 °C, where it was removed, inverted, placed into a centrifuge, and spun for 1 min at 6500 rpm. Finally, the reaction vessel was opened in a N_2 filled drybox equipped with a microscope and at a moisture level < 1 ppm. The crucible in which the elements were placed contained an abundance of multifacetted single crystals of $Eu_{10}Mn_6Sb_{13}$.

Table 1. Selected Data from the Single-Crystal Structure Refinement of $Eu_{10}Mn_6Sb_{13}$

empirical formula	$Eu_{10}Mn_6Sb_{13}$
fw (g/mol)	3431.99
temp (K)	90(2)
wavelength (λ = Mo Kα, Å)	0.710 69
cryst syst	monoclinic
space group	*C*2/*m* (No.12)
unit cell dimens	
a (Å)	15.1791(6)
b (Å)	19.1919 (7)
c (Å)	12.2679(4)
β (deg)	108.078(1)
vol (Å^3)	3397.4(2)
Z	4
density, ρ_{calc} (g/cm^3)	6.710
absorp coeff (mm^{-1})	30.397
reflcns collected	17 443
independent reflcns	3715
final *R* indices [$F_o^2 > 2\sigma(F_o^2)$][a]	R1 = 0.0404; wR2 = 0.0920
R indices ($F_o^2 > 0$)	R1 = 0.0657; wR2 = 0.1032
largest diff. peak and hole (e/Å^3)	7.835 and −3.024

[a] $R1 = \sum||F_o| - |F_c||/\sum|F_o|$. $wR2 = [\sum[w(F_o^2 - F_c^2)^2]/\sum[w(F_o^2)^2]]^{1/2}$; $w^{-1} = [\sigma^2(F_o^2) + (0.0305P)^2 + 28.39P]$, where $P = [\max(F_o^2,0) + 2F_c^2]/3$.

Single-Crystal X-ray Diffraction. All reactions produced a high yield of reflective, silver-colored, multifacetted single crystals with crystal faces ranging in approximate dimensions from 0.1 to 2.0 mm^2. A suitable crystal was selected and cut to the dimensions of 0.02 × 0.007 × 0.009 mm^3. The crystal was coated with Paratone N oil and subsequently mounted on a glass fiber that was placed under a nitrogen cold stream. The single-crystal diffraction data were collected at 90 K using a Bruker SMART 1000 CCD diffractometer employing graphite-monochromatized Mo Kα radiation (λ = 0.710 69 Å). The SMART software was used for data acquisition, the SAINT software for data extraction and reduction, and XPREP v6.12 software for the empirical absorption correction. Initial atomic positions were found by direct methods using XS followed by subsequent difference Fourier syntheses. The refinement was performed by full matrix least-squares methods using SHELXL-97. All atoms were refined with anisotropic thermal parameters except for Sb(7), which was kept isotropic. When the usual anisotropic refinement was applied to this atom, the U_{22} value became very small and would not converge. No model incorporating position disorder for this atom could be found. Since it is the central atom of the linear Sb_3^{5-} unit, one or more vibrational modes that do not fit the 3 × 3 tensor are possibly contributing to this anomaly. Data collection parameters and crystallographic information are provided in Table 1. Positional parameters and isotropic thermal parameters are provided in Table 2. Selected bond distances and angles are listed in Table 3. Complete crystallographic information in the form of a CIF formatted file is provided as Supporting Information.

Magnetic Measurements. DC magnetization data were collected using a Quantum Design MPMS superconducting quantum interference device (SQUID) magnetometer with a 7 T superconducting magnet. Temperature- and field-dependent magnetization measurements of the title compound were obtained by using a 0.0136 g

---

(8) Holmes, S. M.; Girolami, G. S. *J. Am. Chem. Soc.* **1999**, *121*, 5593−5594.

(9) Miller, J. S.; Epstein, A. J. *Chem. Eng. News* **1995**, *73*, 30−41.

(10) Chan, J. Y.; Kauzlarich, S. M.; Klavins, P.; Liu, J.-Z.; Shelton, R. N.; Webb, D. J. *Phys. Rev. B* **2000**, *61*, 459−463.

(11) Chan, J. Y.; Kauzlarich, S. M.; Klavins, P.; Shelton, R. N.; Webb, D. J. *Chem. Mater.* **1997**, *9*, 3132−3135.

(12) Chan, J. Y.; Kauzlarich, S. M.; Klavins, P.; Shelton, R. N.; Webb, D. J. *Phys. Rev. B* **1998**, *57*, 8103−8106.

(13) Kim, H.; Chan, J. Y.; Olmstead, M. M.; Klavins, P.; Webb, D. J.; Kauzlarich, S. M. *Chem. Mater.* **2002**, *14*, 206−216.

(14) Sánchez-Portal, D.; Martin, R. M.; Kauzlarich, S. M.; Pickett, W. E. *Phys. Rev. B* **2002**, *65*, 144414.

(15) Holm, A. P.; Kauzlarich, S. M.; Morton, S. A.; Waddill, G. D.; Pickett, W. E.; Tobin, J. G. *J. Am. Chem. Soc.* **2002**, *124*, 9894−9898.

(16) Hirose, H.; Ueda, K.; Kawazoe, H.; Hosono, H. *Chem. Mater.* **2002**, *14*, 1037−1041.

(17) Köckerling, M.; Johrendt, D.; Finckh, E. W. *J. Am. Chem. Soc.* **1998**, *120*, 12297.

(18) Canfield, P. C.; Fisk, Z. *Philos. Mag. B* **1992**, *65*, 1117−1123.

Table 2. Atomic Coordinates ($\times 10^4$) and Equivalent Isotropic Displacement Parameters (Å^2 $\times$ 10^3) for $Eu_{10}Mn_6Sb_{13}$

atom	Wyckoff position	x	y	z	*U*(eq)[a]
Eu(1)	4h	0	3813(1)	5000	6(1)
Eu(2)	4g	0	3885(1)	0	7(1)
Eu(3)	8j	3203(1)	3816(1)	1708(1)	10(1)
Eu(4)	8j	2366(1)	3819(1)	−1649(1)	9(1)
Eu(5)	8j	2521(1)	3723(1)	4997(1)	6(1)
Eu(6)	4h	5000	3499(1)	0	9(1)
Eu(7)	4g	5000	3643(1)	5000	7(1)
Sb(1)	4i	1662(1)	5000	6309(1)	6(1)
Sb(2)	8j	697(1)	3858(1)	2761(1)	7(1)
Sb(3)	4i	1665(1)	5000	39(1)	6(1)
Sb(4)	8j	1543(1)	2629(1)	0(1)	9(1)
Sb(5)	8j	4324(1)	3430(1)	7257(1)	10(1)
Sb(6)	4i	3538(1)	5000	3840(1)	7(1)
Sb(7)	4i	4327(1)	5000	7346(1)	4(1)
Sb(8)	4i	3992(1)	5000	17(1)	9(1)
Sb(9)	8j	1598(1)	2527(1)	6376(1)	5(1)
Mn(1)	4i	1671(2)	5000	2350(3)	10(1)
Mn(2)	4i	503(2)	5000	−2272(3)	10(1)
Mn(3)	8j	429(2)	2692(1)	7706(2)	10(1)
Mn(4)	8j	1572(1)	2680(1)	2286(2)	10(1)

[a] *U*(eq) is defined as one-third of the trace of the orthogonalized $\mathbf{U}_{ij}$ tensor.

Table 3. Selected Bond Distances (Å) and Angles (deg) in $Eu_{10}Mn_6Sb_{13}$

Mn(1)−Sb(2) ×2	2.776(2)	Eu(3)−Sb(6)	3.3819(12)
Mn(1)−Sb(3)	2.833(3)	Eu(3)−Sb(9)	3.4374(11)
Mn(1)−Sb(6)	2.856(3)	Eu(3)−Sb(4)	3.5568(12)
Mn(2)−Sb(1)	2.832(3)	Eu(3)−Sb(4)	3.5677(11)
Mn(2)−Sb(2) ×2	2.794(2)	Eu(3)−Sb(5)	3.6462(12)
Mn(2)−Sb(3)	2.836(3)	Eu(4)−Sb(3)	3.4532(11)
Mn(3)−Sb(2)	2.765(2)	Eu(4)−Sb(1)	3.3008(12)
Mn(3)−Sb(4)	2.800(2)	Eu(4)−Sb(4)	3.5264(11)
Mn(3)−Sb(5)	2.680(2)	Eu(4)−Sb(4)	3.5322(12)
Mn(3)−Sb(9)	2.777(2)	Eu(4)−Sb(5)	3.6970(11)
Mn(4)−Sb(2)	2.774(2)	Eu(4)−Sb(8)	3.5042(12)
Mn(4)−Sb(4)	2.792(2)	Eu(4)−Sb(9)	3.4088(11)
Mn(4)−Sb(5)	2.679(2)	Eu(5)−Sb(2)	3.2476(12)
Mn(4)−Sb(9)	2.782(2)	Eu(5)−Sb(1)	3.4066(10)
Sb(4)−Sb(4)	2.9486(19)	Eu(5)−Sb(5)	3.2829(12)
Sb(5)−Sb(7)	3.0151(10)	Eu(5)−Sb(6)	3.4308(11)
Sb(8)−Sb(8)	3.074(3)	Eu(5)−Sb(9)	3.4002(10)
Mn(3)−Mn(4)	3.041(3)	Eu(5)−Sb(9)	3.4318(10)
Eu(1)−Sb(2) ×2	3.2367(9)	Eu(6)−Sb(4) ×2	3.1882(12)
Eu(1)−Sb(1) ×2	3.4087(11)	Eu(6)−Sb(5) ×2	3.2019(9)
Eu(1)−Sb(9) ×2	3.5038(11)	Eu(6)−Sb(8) ×2	3.2659(11)
Eu(2)−Sb(3) ×2	3.3013(11)	Eu(7)−Sb(5) ×2	3.2634(9)
Eu(2)−Sb(2) ×2	3.2203(9)	Eu(7)−Sb(6) ×2	3.4318(11)
Eu(2)−Sb(4) ×2	3.3602(11)	Eu(7)−Sb(9) ×2	3.3508(11)
Sb(2)−Mn(1)−Sb(2)	104.32(10)	Sb(2)−Mn(3)−Sb(9)	115.91(8)
Sb(2)−Mn(1)−Sb(3)	110.20(8)	Sb(5)−Mn(3)−Sb(4)	108.43(8)
Sb(2)−Mn(1)−Sb(6)	111.25(8)	Sb(2)−Mn(3)−Sb(4)	112.64(8)
Sb(3)−Mn(1)−Sb(6)	109.53(10)	Sb(9)−Mn(3)−Sb(4)	106.82(8)
Sb(2)−Mn(2)−Sb(2)	103.37(10)	Sb(5)−Mn(4)−Sb(2)	107.23(8)
Sb(2)−Mn(2)−Sb(1)	110.84(8)	Sb(5)−Mn(4)−Sb(9)	103.99(8)
Sb(2)−Mn(2)−Sb(3)	112.12(8)	Sb(2)−Mn(4)−Sb(9)	116.59(8)
Sb(1)−Mn(2)−Sb(3)	107.59(11)	Sb(5)−Mn(4)−Sb(4)	109.38(8)
Sb(5)−Mn(3)−Sb(2)	107.47(8)	Sb(2)−Mn(4)−Sb(4)	112.33(8)
Sb(5)−Mn(3)−Sb(9)	105.12(8)	Sb(9)−Mn(4)−Sb(4)	106.86(8)

single-crystal sample that was initially etched with a 5% HCl in MeOH solution, immediately coated with an N-type Apiezon grease, and placed in a straw. The temperature-dependent data were obtained by measuring zero-field-cooled (ZFC) magnetization from 2 to 300 K and field-cooled (FC) magnetization from 300 to 2 K in applied magnetic fields of 0.1 and 5 T. Field-dependent magnetization data were taken at 2 K by sweeping through fields from 0 to +7, +7 to −7, and −7 to +7 T.

Resistivity Measurements. Temperature-dependent resistivity measurements were obtained on a single crystal (1.0 × 1.5 × 3.0 mm^3) using an in-line four-probe method. A Keithley Model 224 current source and a Keithley 181 nanovoltmeter were used to measure resistivity from 2 to 300 K. A constant current (100 μA) was applied to the sample through the two outer leads, and the voltage was measured across the two inner leads. Thermal voltages were minimized by reversal of the current bias. The sample surface used for the measurements was prepared by etching the crystal using a 5% HCl in MeOH solution followed by polishing a surface to a highly reflective finish. Pt leads were immediately attached by Ag paint and cured by resistive heating. The sample exhibited ohmic behavior. Resistivity as a function of temperature was also measured with applied fields of 1, 2, and 5 T in the temperature range 10−60 K.

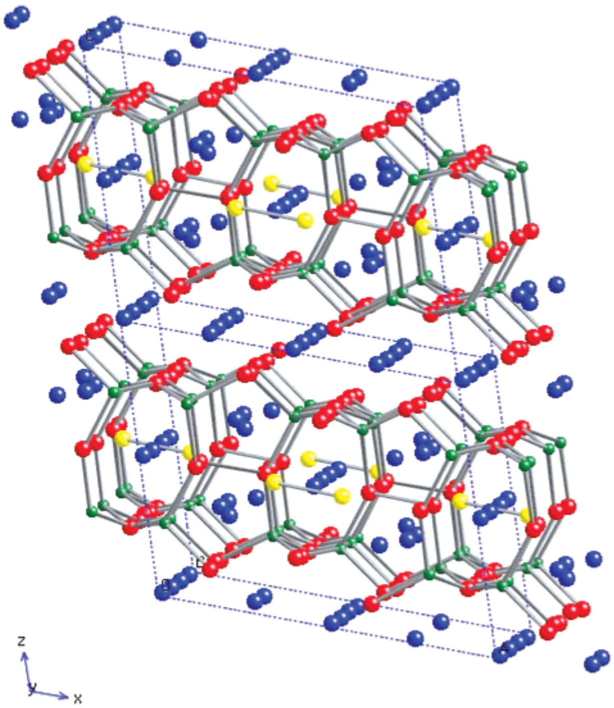

Figure 1. View of the crystal structure of $Eu_{10}Mn_6Sb_{13}$ down the *b* axial direction showing the unit cell outline. Eu is blue, Sb is red, $[Sb]^{2-}$ dimers are yellow, and Mn is green.

Mössbauer Spectral Measurements. The ^{151}Eu Mössbauer spectra were obtained on a constant-acceleration spectrometer which utilized a SmF_3 source. The isomer shifts are reported relative to EuF_3 at room temperature with an estimated error of ±0.05 mm/s. The velocity scale was calibrated at room temperature with a cobalt-57 source and an α-iron absorber. The absorber, which contained 60 mg/cm^2 of powdered sample mixed with boron nitride, was prepared and maintained under a dry nitrogen atmosphere.

Results and Discussion

Structure Description. Figure 1 shows a representation of the crystal structure of $Eu_{10}Mn_6Sb_{13}$ down the *b* axis direction. The structure is made up of slabs of $[Eu_6Mn_6Sb_{13}]^{8-}$ separated by planes of Eu ions. The complex layers have a covalent Mn/Sb network of edge-sharing and corner-sharing Mn-centered tetrahedra, layers which accommodate additional Eu ions in their cavities. The slabs exhibit identifiable blocks of $[Mn_{12}Sb_{24}]^{36-}$ clusters. This 12-membered tetrahedral anionic cluster, $[Mn_{12}Sb_{24}]^{36-}$, zigzags in the *ab* plane to form holes that are occupied by Eu^{2+} ions, isolated $[Sb_2]^{4-}$ dumbbell anions, and a bridging Sb atom that acts to link

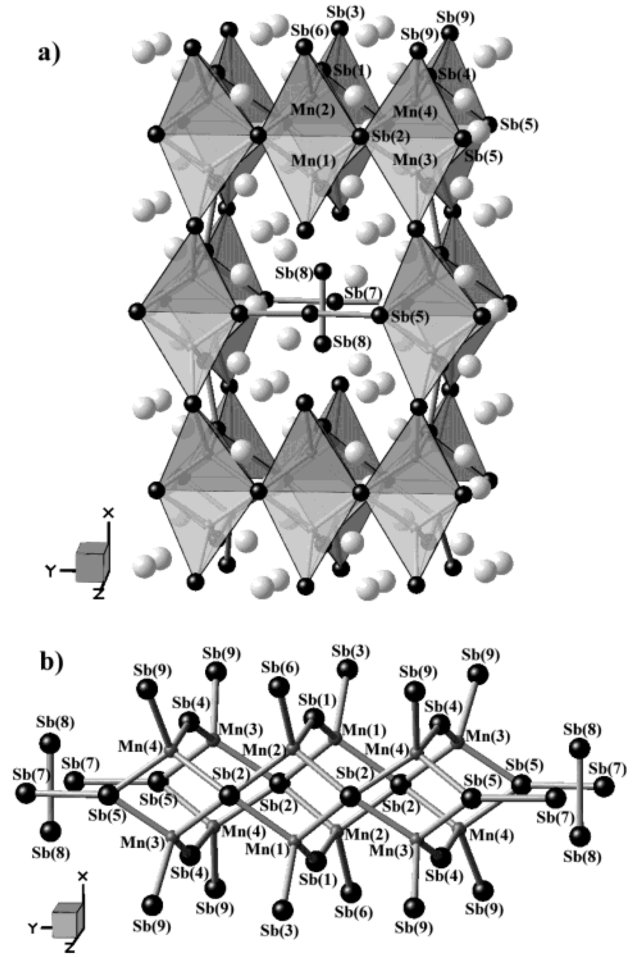

Figure 2. (a) View showing the channel filled with isolated dumbbells and Eu^{2+} atoms. (b) Detailed basic building motif $[(Mn_{12}Sb_{24})^{36-}(Sb_2)^{4-}]^{40-}$ composed of two $[Mn_6Sb_{12}]^{18-}$ anions and the isolated $[Sb_2]^{4-}$ dumbbell anions at the end of the building motif. Eight Sb(5) and four Sb(8) atoms and two Sb_2 dumbbells are shared by neighbors to make the building motif $[(Mn_{12}Sb_{18}Sb_{12/2})^{36-}(Sb_2)^{4-}]^{40-}$.

two other Sb atoms belonging to two different $[Mn_{12}Sb_{24}]^{36-}$ clusters forming linear $[Sb_3]^{5-}$ trimers. Figure 2 shows a representation of a slab fragment displaying a channel filled with isolated Sb(8)−Sb(8) dumbbells and Eu^{2+} atoms. Rows of Eu atoms extend through these channels down the *a* and *b* axial directions. Figure 2b shows details of the basic building motif, $[(Mn_{12}Sb_{24})^{36-}(Sb_2)^{4-}]$,$^{40-}$ which is composed of two edge and corner sharing $[Mn_6Sb_{12}]^{18-}$ units that lie side-by-side to form the $[Mn_{12}Sb_{24}]^{36-}$ component. Isolated $[Sb_2]^{4-}$ dumbbell anions with a Sb−Sb distance of 3.074(3) Å are found at the two ends of this building block. The dumbbells are situated in the cavity between the two bridging $[Sb_3]^{5-}$ trimers, defined by Sb(5)−Sb(7)−Sb(5). The distances of 3.0151(10) Å found for Sb(5)−Sb(7) are similar to those observed for the $[Pn_3]^{7-}$ linear anionic unit found in compounds with the $Ca_{14}AlSb_{11}$ structure type.[19] The formula can be best described as $(40Eu^{2+})(2[Mn_{12}Sb_{24}]^{36-}2[Sb_2]^{4-})$,$^{80-}$ where $2[Sb_2]^{4-}$ represents two isolated $[Sb_2]^{4-}$ dumbbells per unit cell and the $[Sb_3]^{5-}$ trimers and bridging $[Sb_2]^{4-}$ dumbbell anions are included in the $[Mn_6Sb_{24}]^{36-}$ anion.

The distance of the Sb(8)−Sb(8) bond in the dumbbell anion is 3.074(3) Å, slightly larger than the average single-bond length for compounds containing this structural unit, i.e., 2.844 Å in $Sr_{21}Mn_4Sb_{18}$,[20] 2.866 Å in $Ca_{21}Mn_4Sb_{18}$,[21] and 2.84 Å in $Ca_{11}InSb_9$,[22] but it is within reason to describe this bond as a single Sb−Sb bond. Figure 3 shows local geometries of the seven different Eu atoms. The Eu atoms that separate the $[Eu_6Mn_6Sb_{13}]^{8-}$ slabs are Eu(1), Eu(5), and Eu(7), and they adopt octahedral coordination environments defined by Sb atoms. The Eu atoms found inside the slabs adopt both trigonal prismatic and octahedral coordination. Bond distances and angles for the Eu atoms are given in Table 3.

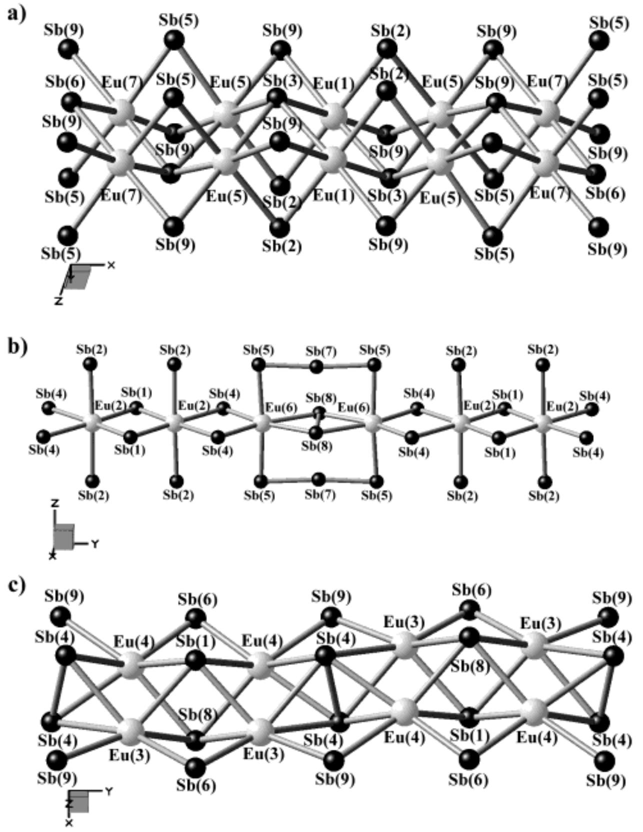

Figure 3. Local coordination environment of Eu in $Eu_{10}Mn_6Sb_{13}$: (a) Eu(1), Eu(5), and Eu(7), showing octahedral geometry; (b) Eu(2) and Eu(6), showing octahedral geometry, and (c) Eu(3) and Eu(4), which are in the most distorted geometry.

The Mn−Sb bond lengths range from 2.679(2) to 2.856(3) Å. These Mn−Sb bond distances are in good agreement with the previously reported ternary manganese antimonide compounds of $EuMn_2Sb_2$ (2.758 Å),[23] $BaMnSb_2$ (2.804 Å),[24] $Ca_{14}MnSb_{11}$ (2.759 Å),[25] $Sr_{21}Mn_4Sb_{18}$ (2.763−3.007 Å),[20] and $Ca_{21}Mn_4Sb_{18}$ (2.717−2.854 Å).[21] The Sb−Mn−Sb bond angles of the tetrahedra show small deviations from the ideal tetrahedral angle of 109.5° as is observed throughout the $[Mn_{12}Sb_{24}]^{36-}$ unit with the maximum angle of 116.59(8)°

---

(19) Cordier, G.; Schäfer, H.; Stelter, M. *Z. Anorg. Allg. Chem.* **1984**, *519*, 183−188.

(20) Kim, H.; Condron, C. L.; Holm, A. P.; Kauzlarich, S. M. *J. Am. Chem. Soc.* **2000**, *122*, 10720−10721.

(21) Holm, A. P.; Olmstead, M. M.; Kauzlarich, S. M. *Inorg. Chem.* **2003**, *42*, 1973−1981.

(22) Cordier, G.; Schäfer, H.; Stelter, M. *Z. Naturforsch.* **1985**, *40b*, 868−871.

(23) Ruehl, R.; Jeitschko, W. *Mater. Res. Bull.* **1979**, *14*, 513−517.

(24) Cordier, G.; Schäfer, H. *Z. Naturforsch.* **1977**, *32 b*, 383−386.

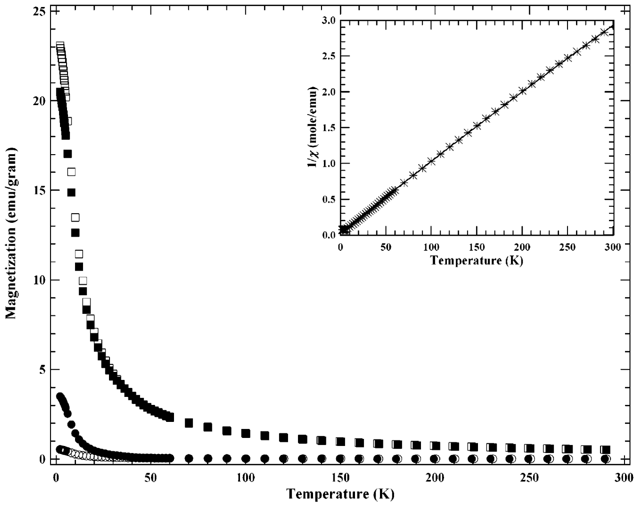

Figure 4. Magnetization vs temperature for $Eu_{10}Mn_6Sb_{13}$. Circles are 0.1 T and squares are 5 T measurements. The filled symbols are FC, and the open symbols are ZFC measurements. The inset shows the inverse susceptibility obtained at $H = 5$ T vs temperature for the ZFC measurement. The solid line in the inset is the least-squares fit to the inverse susceptibility vs temperature for the data collected at $H = 5$ T.

occurring between Sb(2)−Mn(4)−Sb(9), and the minimum angle of 103.37(10)° occurring between Sb(2)−Mn(2)−Sb(2). The distances between neighboring Mn atoms, Mn(1)−Mn(2) (3.272(2) Å) and Mn(3)−Mn(4) (3.041(3) Å) are long. The nearest Mn−Mn distance is similar to that of $Sr_{21}Mn_4Sb_{18}$ with 2.932 Å.[20]

According to the Zintl formalism, the formal charge of four-bonded Sb(2) atoms can be assigned as Sb^+, of three-bonded Sb(4) and Sb(5) as Sb^0, of two-bonded Sb(1), Sb(7), and Sb(9) as Sb^-, and of one-bonded Sb(3), Sb(6), and Sb(8) as Sb^{2-}. The use of the formal charge reflects the viewpoint that the bonding between Mn and Sb atoms in the anionic framework is covalent. Because the chemical behavior of Mn^{2+} is very similar to that of Zn^{2+} in other Zintl phases, for electron counting purposes, the Mn atoms in $Eu_{10}Mn_6Sb_{13}$ may be substituted with Zn atoms; i.e., the d^5 electrons are ignored. Examples of Mn and Zn isostructural compounds are RE_6MnSb_{15}−RE_6ZnSb_{15}, where RE is La, or Ce.[26] Therefore, this compound can be considered as valence precise and can be described as $(Eu^{2+})_{40}(Mn^{2-})_{24}(4bSb^+)_8(3bSb^0)_{16}(2bSb^-)_{16}(1bSb^{2-})_{12}$.

Physical Properties. *Magnetic Susceptibility Measurements.* Figure 4 shows the magnetization of $Eu_{10}Mn_6Sb_{13}$ as a function of temperature for measurements taken with applied fields of 0.1 and 5 T. As expected, the lower value magnetization corresponds to the low-field measurement. The low-field results show a pronounced divergence between ZFC and FC measurements at ~42 K. This effect is less pronounced though still present in the high-field results. The inset in Figure 4 shows the 5 T inverse susceptibility as a function of temperature together with a least-squares fit. The shape of the inverse susceptibility versus temperature curve indicates Curie−Weiss type behavior in the high-temperature region. The fit was carried out with a modified Curie−Weiss model, $\chi = (C/(T - \theta)) + \chi_0$, with $C = 97.5(7)$ emu·K/mol, $\chi_0 = 0.019(2)$ emu/mol, and $\theta = -2.2(3)$ K. An effective moment of 27.9(1) μ_B is obtained from the equation $\mu_{eff} = \sqrt{7.99C}$ and is only slightly reduced from the expected effective moment of 29.0 μ_B based on 10 Eu^{2+} and 6 Mn^{2+} ions and calculated using the spin-only moments of $\mu_{Eu2+} = 7.94\mu_B$ and $\mu_{Mn2+} = 5.92\mu_B$. The Weiss constant of −2.2 K is very small and suggests very weak low-temperature antiferromagnetic interactions. The ferromagnetic component observed in Figure 4 suggests that some of the Eu^{2+} cations are undergoing magnetic ordering below 50 K, an ordering which is indeed observed in the Mössbauer spectra; see below. Figure 5 shows the $M(H)$ data obtained at 2 K and shows no measurable hysteresis. The maximum magnetization value at 7 T of ~50 μ_B/(formula unit) is much lower than the ~100 μ_B expected for 10 Eu^{2+} and 6 Mn^{2+} ions. Even neglecting the Mn^{2+} moments which are likely to be antiferromagnetically coupled, there is still a reduction in the moment expected for 10 Eu^{2+} ions. This reduction could be the result of incomplete saturation of the moments at 7 T.

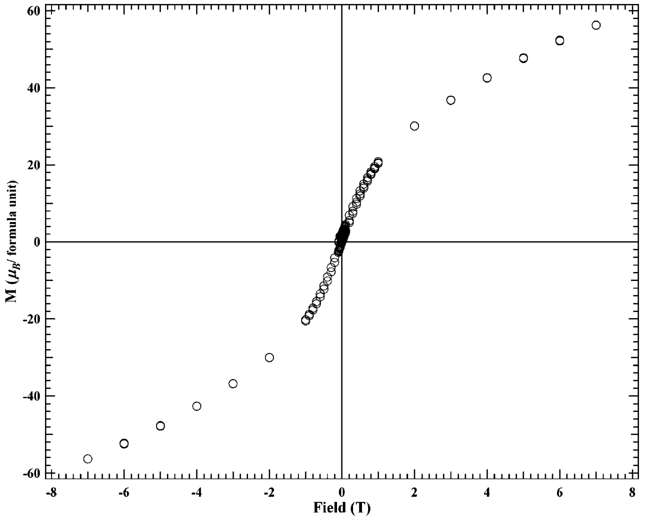

Figure 5. Magnetization vs applied field for $Eu_{10}Mn_6Sb_{13}$ obtained at 2 K.

Charge Transport Properties. Figure 6 shows the resistivity as a function of temperature measured for a single crystal of $Eu_{10}Mn_6Sb_{13}$. The room-temperature resistivity value is 7.04(9) Ω·cm. The top inset shows the resistivity measured in different applied magnetic fields between 10 and 60 K. The bottom inset is a plot of ln ρ vs $1/T$ between 100 and 300 K. At high temperature, the resistivity shows a temperature dependence typical of semiconductors. The plot of ln ρ vs $1/T$ is nearly linear between 100 and 300 K, and an activation energy of 0.115(2) eV is calculated from the equation, $\ln \rho = (E_a/2k_BT) - \ln \rho_o$. However, below approximately 60 K, there is a significant rise in resistivity which reaches a maximum at ~40 K and then decreases upon cooling to ~10 K; below ~10 K the resistivity begins to rise slightly again. The applied magnetic field has no effect on the resistivity data above ~42 K, but there is a slight increase

---

(25) Rehr, A.; Kuromoto, T. Y.; Kauzlarich, S. M.; Del Castillo, J.; Webb, D. J. *Chem. Mater.* **1994**, *6*, 93−99.

(26) Sologub, O.; Vybornov, M.; Rogl, P.; Hiebl, K.; Cordier, G.; Woll, P. *J. Solid State Chem.* **1996**, *122*, 266−272.

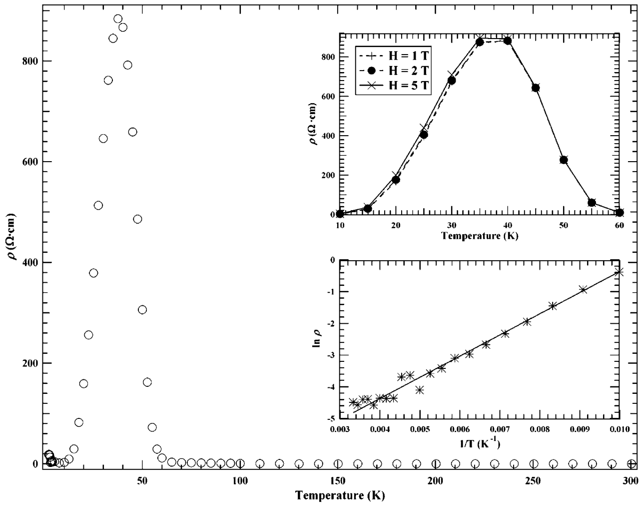

Figure 6. Resistivity vs temperature of $Eu_{10}Mn_6Sb_{13}$. The lower inset shows the ln ρ vs (temperature)$^{-1}$ and the least-squares fit to that data. The upper inset shows the resistivity as a function of temperature from 10 to 60 K at applied fields of 1, 2, and 5 T.

in resistivity with increasing field upon cooling to ~15 K with the 5 T data showing the most significant change.

Mössbauer Spectroscopy. The ^{151}Eu Mössbauer spectra of $Eu_{10}Mn_6Sb_{13}$, obtained between 4.2 and 60 K and at 100 and 295 K, are shown in Figures 7 and 8, respectively. Because the resolution of europium-151 Mössbauer spectroscopy is limited by its typical line width of 2.3 mm/s, it is difficult to analyze the Mössbauer spectra with seven different components assigned to the seven crystallographically inequivalent europium sites, sites that mostly have very similar pseudooctahedral antimony coordination environments. To reduce the number of components used to fit the spectra, the europium sites have been divided into three groups with relative degeneracies of 16:20:4 corresponding, first, to the Eu(2) 4*g*, Eu(5) 8*j*, and Eu(1) 4*h* sites with Wigner−Seitz cell volumes[27] of 44.08, 44.39, and 45.40 Å^3, respectively, second, to the Eu(7) 4*g*, Eu(4) 8*j*, and Eu(3) 8*j* sites with volumes of 43.31, 43.32, and 43.62 Å^3, respectively, and, third, to the Eu(6) 4*h* site with a volume of 39.80 Å^3. The Wigner−Seitz cell volumes have been calculated[27] by using 12 coordinate metallic radii of 1.99, 1.35, and 1.59 Å for Eu, Mn, and Sb, respectively. Hence, three components, all with the same line width of 2.3 mm/s and with relative areas of 16:20:4 or 4:5:1, have been used to fit the spectra obtained between 4.2 and 295 K.

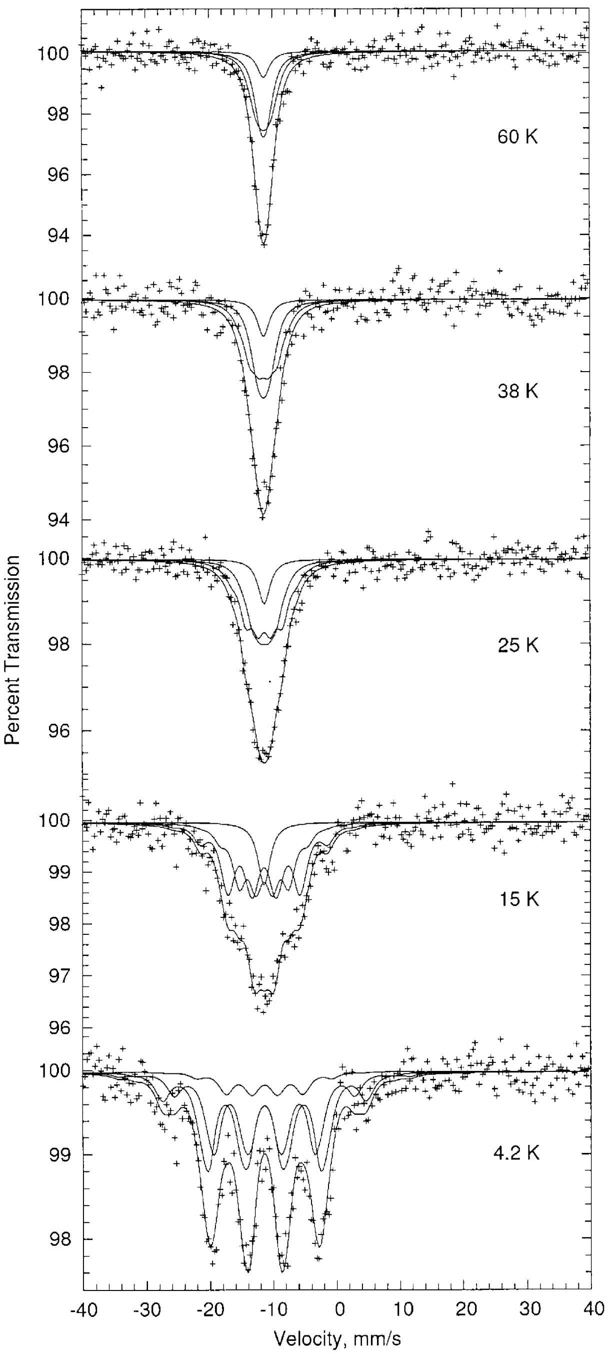

Figure 7. ^{151}Eu Mössbauer spectra of $Eu_{10}Mn_6Sb_{13}$ measured between 4.2 and 60 K.

The spectra of $Eu_{10}Mn_6Sb_{13}$ observed at 4.2 and 15 K, see Figure 7, contain enough information to be unequivocally analyzed with three spectral components. At 4.2 K the spectrum has been fit with three magnetically split components, i.e., three 18 line components, whose hyperfine parameters are given in Table 4. One isomer shift for each of the three components has been adjusted, but the quadrupole interaction has been constrained to zero for each of the components because there is no measurable asymmetry in the observed spectrum. The resulting hyperfine field, H_6, corresponds to Eu(6); H_{125}, corresponds to Eu(1), Eu(2), and Eu(5); and H_{347}, corresponds to Eu(3), Eu(4), and Eu(7): $\langle H \rangle$ is the weighted average of these three fields. With this assignment, the hyperfine fields increases with the Wigner−Seitz cell volume as is observed[28] in many iron−rare-earth intermetallic compounds. Although somewhat smaller than usual, the three hyperfine fields are typical of divalent europium.[29] The 15 K spectrum exhibits a strong central absorption at ca. −11 mm/s, an absorption which cannot be fit unless a component with a zero hyperfine field, i.e., a

---

(27) Gelato, L. *J. Appl. Crystallogr.* **1981**, *14*, 141−142.

(28) Grandjean, F.; Long, G. J. In Interstitial Intermetallic Alloys; Grandjean, F., Long, G. J., Buschow, K. H. J., Eds.; Kluwer Academic Publishing: Dordrecht, 1995; pp 463−496.

(29) Grandjean, F.; Long, G. J. In *Mössbauer Spectroscopy Applied to Inorganic Chemistry*; Long, G. J., Grandjean, F., Eds.; Plenum Press: New York, 1989; Vol. 3, pp 513−597.

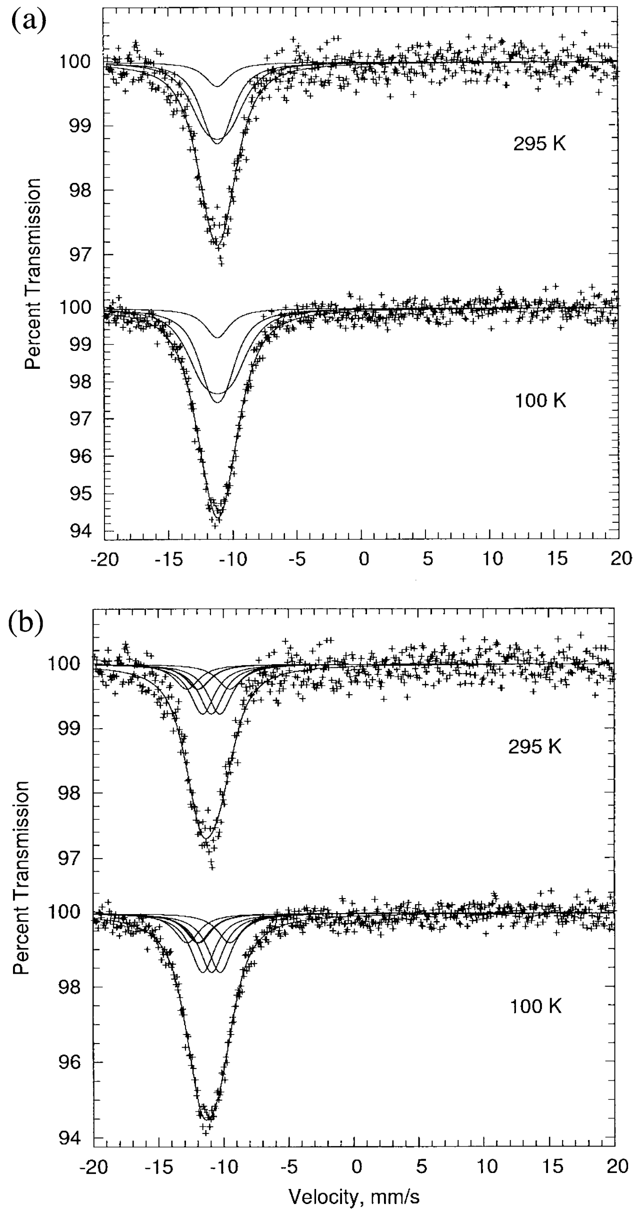

Figure 8. ^{151}Eu Mössbauer spectra of $Eu_{10}Mn_6Sb_{13}$ measured at 100 and 295 K, fitted with three components (a) and with seven singlets (b).

Table 4. Europium-151 Mössbauer Spectral Hyperfine Parameters

T (K)	δ^a (mm/s)	$\langle H \rangle$ (T)	H_6 (T)	H_{125} (T)	H_{347} (T)	area (%ϵ) (mm/s)
295	−11.2(1)	2.0(3)	0	1.4(5)	2.9(5)	13.7(2)
100	−11.2(1)	2.3(3)	0	1.7(5)	3.4(5)	28.7(2)
60	−11.3(1)	2.2(3)	0	1.6(5)	3.2(5)	35(1)
38	−11.4(1)	3.7(3)	0	2.6(5)	5.3(5)	40(1)
25	−11.3(1)	5.3(2)	0	4.5(3)	7.0(3)	41(1)
15	−11.4(1)	10.7(2)	0	9.5(3)	13.9(3)	48(1)
4.2	−11.3(1)	20.5(2)	15(1)	19.7(3)	22.2(3)	48(1)

[a] Relative to room-temperature EuF_3.

singlet, is introduced into the model. Hence, the spectral results indicate that the Eu(6) magnetic moments are not ordered at 15 K, whereas the other europium magnetic moments are ordered. This assignment is based on the relative area, the small field at 4.2 K, and the small Wigner−Seitz cell volume of the Eu(6) site. To show the uniqueness of this fitting model and, more specifically, the presence of the singlet, a fit of the 15 K spectrum with one magnetically split component was attempted and is shown, together with the fit with three components, in Figure 9. A comparison of the two fits and the squared residuals indicates that the fit using the singlet is significantly better.

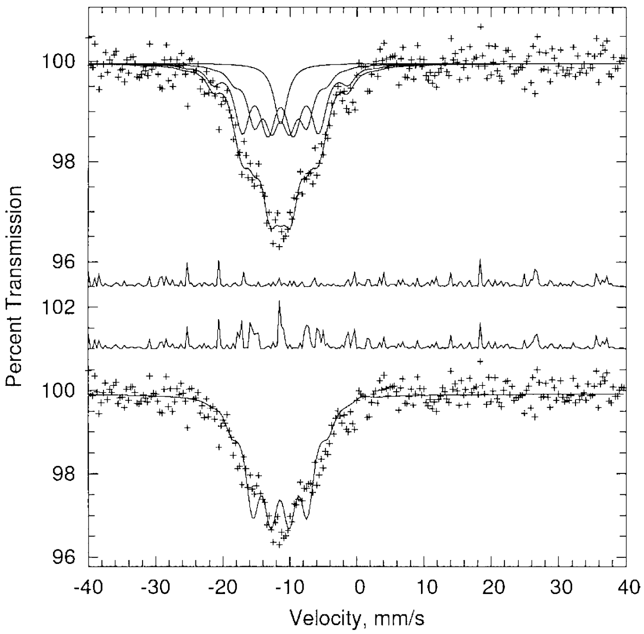

Figure 9. Mössbauer spectrum at 15 K of $Eu_{10}Mn_6Sb_{13}$ fit with three components (top) and with one magnetic component (bottom). The fit residuals for the respective fits are shown in the center.

The same model with two magnetically split components and one singlet component has been used to fit the spectra above 15 K (see Figures 7 and 8a), and the corresponding hyperfine parameters are given in Table 4. Because the spectra at 100 and 295 K are obtained in the temperature region where the compound exhibits a paramagnetic susceptibility, their analysis with two weak hyperfine fields for six of the seven europium sites may be difficult to justify. An alternative fit with seven singlets, with relative areas constrained to the europium site degeneracies and a line width of 2.3 mm/s, is shown in Figure 8b. These fits are clearly, as expected, excellent but the 3.3 mm/s range of isomer shifts from −12.7 to −9.4 mm/s observed for the seven europium sites at 100 and 295 K is rather large for divalent europium sites with very similar coordination environments. The inherent resolution of the ^{151}Eu Mössbauer spectra does not permit a choice between the two fitting models, but the three-component model discussed above is preferred because it yields a consistent analysis of the spectra as a function of temperature.

The observed isomer shift of −11.2(1) mm/s is characteristic[29] of divalent europium and, within the error limits, is independent of temperature. Samuel and Delgass[30] have shown that hybridization of the 4f electrons with the 6s electrons will affect the ^{151}Eu isomer shift. Specifically, the $4f^7 6s$ electronic configuration has an isomer shift that is ca. 6 mm/s greater than that of the free-ion europium(II) $4f^7$ electronic configuration. Further, there is a positive difference[30] of ca. 10 mm/s between the isomer shifts of the $4f^7$ and $4f^6$ electronic configurations. The positive difference

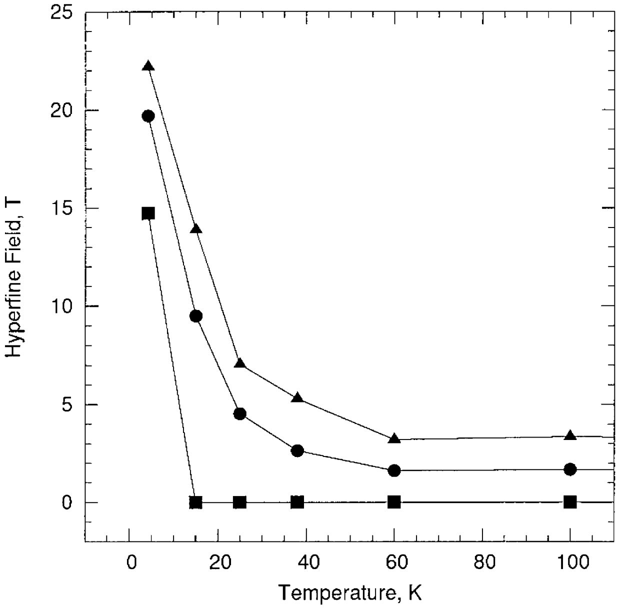

Figure 10. Temperature dependence of the H_6 (▲), H_{125} (●), and H_{347} (■), ^{151}Eu Mössbauer spectral hyperfine fields observed in $Eu_{10}Mn_6Sb_{13}$.

between the −11.2 mm/s average isomer shift measured herein and the −13.5 mm/s isomer shift observed[30] for EuF_2 represents a gain of 0.37 6s electrons or a loss of 0.22 4f electrons. Thus in $Eu_{10}Mn_6Sb_{13}$ the average electronic configuration of europium is between $4f^7 6s^{0.37}$ and $4f^{6.78}$ plus 2.22 conduction electrons, configurations that are consistent with a formal +2 oxidation state for europium.

The −11.2(1) mm/s isomer shift observed for $Eu_{10}Mn_6Sb_{13}$, in which the europium is bonded only to antimony, is very similar to the −11.8 mm/s value observed[31] for $EuFe_4Sb_{12}$ in which the europium is also bonded only to antimony. Further, the −11.2(1) mm/s value is in the −10.7 to −11.4 mm/s range of isomer shifts recently observed[32] for the ternary europium containing pnictides, LiEuPn, where Pn is P, As, Sb, and Bi.

The temperature dependence of the Mössbauer spectral hyperfine fields observed for the three groups of europium ions is shown in Figure 10. At 60, 100, and 295 K, the Eu(6) site exhibits no hyperfine field and the remaining europium ions exhibit very small hyperfine fields of at most 1.5 and 3 T, fields which may be transferred hyperfine fields from the antiferromagnetically ordered Mn next nearest neighbors. At 15, 25, and 38 K, the Eu(6) site does not exhibit a hyperfine field, whereas the field on the other europium sites increases dramatically with decreasing temperature; see Figure 10. Below 40 K the Mössbauer spectra indicate the magnetic ordering of six of the seven europium sites, an ordering that reduces the spin-disorder electron scattering and hence the resistivity; see Figure 6. As long-range magnetic ordering is established upon cooling from 60 to 40 K, the resistivity increases due to spin-disorder scattering. At 4.2 K, all seven europium sites are magnetically ordered as indicated by the three nonzero hyperfine fields (see Figure 10) and by the magnetization (see Figure 5).

Conclusions

$Eu_{10}Mn_6Sb_{13}$ is a new addition to the family of transition-metal Zintl compounds. Formal electron counting suggests that Mn is present as Mn^{2+}, and research is currently underway to confirm this through the preparation of the zinc analogue, $Eu_{10}Zn_6Sb_{13}$.

^{151}Eu Mössbauer spectra indicate that europium is present as Eu^{2+} ions, ions that dominate the magnetic properties of $Eu_{10}Mn_6Sb_{13}$. Further, the Mössbauer spectra indicate that $Eu_{10}Mn_6Sb_{13}$ is probably paramagnetic above 50 K and that six of the seven europium sites are magnetically ordered below 40 K. This ordering is consistent with the observed rise in magnetization and the deviation between the FC and ZFC magnetization and the large anomaly in the resistivity observed at 40 K. Finally, in agreement with the magnetization observed at 2 K, the 4.2 K Mössbauer spectrum shows that all seven europium sublattices are magnetically ordered. The lower ordering temperature of the Eu(6) sublattice may be related to differences in the Eu(6) bonding to antimony and the consequent differences in the exchange coupling in this sublattice as compared with the other sublattices. Further, the lower ordering temperature of the Eu(6) sublattice may account for the very large anomaly observed in the resistivity. The magnetic ordering of different europium sublattices at different temperatures within one compound is unusual, but can be observed through ^{151}Eu Mössbauer spectroscopy, a technique which can distinguish between the magnetic properties of the different europium sublattices. Unfortunately, the Mössbauer spectra do not provide any information on the ferromagnetic or antiferromagnetic ordering of the europium magnetic moments. In principle, neutron diffraction experiments on $Eu_{10}Mn_6Sb_{13}$ could provide such information on the europium magnetic moments but would require the use of a very expensive europium-153 enriched sample.

Acknowledgment. The authors thank Prof. Alan F. Williams of the University of Geneva for the use of the SmF_3 source. This research was funded by the National Science Foundation (Grants DMR-9521739, 9803074, 0120990, and INT-9815138). S.-J.K. and M.G.K. acknowledge financial support from Korea Research Foundation Grant KRF-2001-042-D00054. M.G.K. also thanks the Department of Energy for financial support. A.P.H. was funded by the Materials Research Institute through LLNL. F.G. acknowledges with thanks the financial support of the “Fonds National de la Recherche Scientifique, Belgium” for Grant 9.4565.95. G.J.L. would like to thank the Francqui Foundation of Belgium for his appointment as the Internation Francqui Chair in Liege, Belgium, during 2003.

Supporting Information Available: Crystallographic data is provided in CIF format. This material is available free of charge via the Internet at http://pubs.acs.org.

IC034054W

---

(30) Samuel, E. A.; Delgass, W. N. In *Mössbauer Effect Methodology*; Gruverman, I. J., Seidel, C. W., Eds.; Plenum Press: New York, 1976; p 261.

(31) Bauer, E.; Berger, S.; Galatanu, A.; Galli, M.; Michor, H.; Hilscher, G.; Paul, C.; Ni, B.; Abd-Elmeguid, N. M.; Tran, V. H.; Grytsiv, A.; Rogl, P. *Phys. Rev. B* **2001**, *63*, 224414.

(32) Prill, M.; Mosel, B. D.; Müller-Warmuth, W.; Albering, J.; Ebel, T.; Jeitschko, W. *Solid State Sci.* **2002**, *4*, 695−700.